A triple axis double crystal multiple reflection camera for ultra small angle X-ray scattering

Jacques Lambard, Pierre Lesieur, Thomas Zemb

Classification
Physics Abstracts
61.10F — 78.70V — 82.70

A triple axis double crystal multiple reflection camera for ultra small angle X-ray scattering

Jacques Lambard, Pierre Lesieur and Thomas Zemb

CEA, CEN Saclay, Service de Chimie Moléculaire, BP 125, F91191 Gif-sur-Yvette Cedex, France

(*Received 18 November 1991, accepted 10 January 1992*)

Résumé. — L'extension du domaine de diffusion des rayons-X vers les petits angles demande l'emploi de cristaux à réflexions multiples pour collimater le faisceau. Nous décrivons une caméra à rayons-X à trois axes où les réflexions multiples sont réalisées dans deux cristaux à gorge. Nous donnons ensuite les procédures de déconvolution pour obtenir la section efficace de diffusion en échelle absolue, ainsi que les résultats des mesures effectuées avec plusieurs échantillons typiques : fibres de collagène, sphères de silice de 0,3 μm de diamètre, sphères de latex de 0,16 μm de diamètre en interaction, charbon lignite poreux, cristaux liquides formés dans un système eau-tensioactif, solution colloïdale de sphères de silice de 0,32 μm de diamètre.

Abstract. — To extend the domain of small angle X-ray scattering requires multiple reflection crystals to collimate the beam. A double crystal, triple axis X-ray camera using multiple reflection channel cut crystals is described. Procedures for measuring the desmeared scattering cross-section on absolute scale are described as well as the measurement from several typical samples : fibrils of collagen, 0.3 μm diameter silica spheres, 0.16 μm diameter interacting latex spheres, porous lignite coal, liquid crystals in a surfactant-water system, colloidal crystal of 0.32 μm diameter silica spheres.

1. Introduction.

Small angle X-ray scattering, pioneered by Guinier [1] in alloys fifty years ago allows the study of electron density inhomogeneities of colloidal size, i.e. from 5 to 500 Å. Much larger objects can be directly observed under an optical microscope. However, there remains an intermediate size range, between 500 Å and 5 000 Å where optical as well as small angle X-ray scattering are extremely difficult. Efforts have been made to extend the range of applicability of small-angle X-ray scattering (SAXS) to ultra small angles (USAXS) by developing high resolution cameras. We describe here the solution chosen in our laboratory to build such a camera as well as some illustrative examples.

To obtain useful USAXS data from a colloidal sample, two conditions have to be fulfilled [2] :

— get a minimum momentum q_{min} as small as possible, for which the scattering originated by the sample can be distinguished from the direct beam, thus increase the resolution by decreasing the angular divergence of the beam passing through the sample, at least in one direction ;

— still optimize the flux through the sample and reduce as much as possible any parasitic scattering coming from the tails of the reflection curve of the monochromator as well as from surface scattering on the crystal faces.

The idea of using angular collimation performed with crystals isntead of slits seems to have been proposed for the first time by Compton in 1917 [3]. The theory was established by Compton and Allison in 1935 [4]. The first striking experimental result obtained by this method seems to be the measure of the rocking curve width of calcite crystals in 1921 by Davis and Stempel [5]. In 1926, Slack used the double crystal technique to measure the rocking curve enlargement due to graphite mosaicity [6]. Fankuchen [7] and Dumond [8] used this technique independently to obtain high resolution. Beeman, Kaesberg and Ritland used double crystal techniques in order to measure small angle X-ray scattering of fibers [9-10].

Until 1950, the double crystal techniques could never compete with arrangements using slits and curved crystals introduced by Guinier [11]. The main reason is the strong « tail » of parasitic scattering which is still coming through the camera without sample when the angle between the analyser and monochromator crystalline planes are tilted of the order of minutes of arc : this parasitic scattering is larger than with slits and focusing crystal arrangements, thus hiding weak small angle scattering coming from the sample.

In 1965, the crucial step forward came from Bonse and Hart using triple and fivefold reflections possible on channel-cut crystal [12-13]. These crystals reduce the parasitic tails of the outgoing beam by several orders of magnitude, hence being competitive with arrangements using slits for scattering angles of the same order of magnitude as beam divergence. This beam divergence is set by the monochromator material, such as defectless Ge or Si crystals which became easily available in the last twenty years. We think now that for Bragg spacings larger than 600 Å, the double crystal multiple reflection spectrometer allows easier measurements than a design involving very high collimation with thin slits and a beam stop.

Several other high resolution X-ray multiple crystal cameras have been described in the literature : in Japan for the study of imperfections in nearly perfect crystals by Iida [14] and for the study of Kr bubbles in amorphous and crystalline $Ni_{84}Y_8Kr_8$ by Ratag [15] ; in USSR for the study of the perfection of Si crystals by Koval'chuk [16] ; in the USA by Koffman for metallurgical studies [17] and by Als-Nielsen *et al.* to study smectic thermotropic and diluted lyotropic lamellar phases [18] ; in Denmark to study various X-ray optical elements for astronomy by Christensen [19] and in U.K. mainly for the study of muscle structure by Nave [20] and Bordas [21] or for the study of crystals distorted by epitaxy by Fewster [22].

Last but not least, the single pinhole collimated multiple reflection spectrometer using a crossed arangement of crystals has been described by Bonse and Hart [13], and more recently by Bonse and Pahl [23-25].

2. The multiple crystal multiple reflection camera.

2.1 PRINCIPLE OF THE CAMERA. — The most commonly used experimental setups are limited by the angular size of the beam covering the image of the X-ray source in the detector plane. To obtain a minimum q value $q_{min} = 4\ \pi/\lambda\ \sin\ \theta$ (where λ is the wavelength of radiation and $2\ \theta$ the scattering angle) for heterogeneities of size $\xi = 5\ 000$ Å i.e. $q = \pi/\xi = 6 \times 10^{-4}$ Å^{-1}, one has to reach a minimum angle about 100 μrad with copper Kα radiation. For a reasonable beam-stop size of 5 mm this leads to increase the sample to detector distance up to

25 m. This can be done only with a synchrotron source since such a size prohibits the installation in a laboratory setup using an isotropic source (rotating anode). Keeping the sample-to-detector distance to 1 m, the beam stop size would be reduced to 200 μm. If we remember that near the beam stop edges the intensity is less than 10^{-3} that of the maximum of the beam, one is led to build a micro-focus camera, and to reduce any source of the tails of the beam besides the beam stop.

Detailed experimental aspects of the performances of SAXS cameras using the focusing monochromators pioneered by Guinier are discussed in standard textbooks [11, 26].

A clever setup has been proposed using angular analysis of the outcoming beam instead of a position sensitive detector and a beam stop [7-10, 12, 13]. This camera without beam stop uses a multiple reflection channel cut crystal as monochromator and a second identical crystal to analyse the scattered light [13]. The divergence of the incident beam is fixed by the monochromator and the angular width used for detection is given by the width of the reflection curve of the analyser. Since a Bragg reflection has a very small acceptance angle, a very high resolution is obtained.

The reflection curve $R(\Theta)$ of a planar crystal near a Bragg reflection has roughly the shape of a Lorentzian function. The real curve is given by the dynamic theory of scattering. It is non symmetrical and the tails follow roughly a $(\Theta - \Theta_B)^{-2}$ law. Its expression depends on a few parameters relative to the material and to the order of the reflection [12, 27-28]. With copper Kα radiation, the full width at half maximum of the reflection curve is 35 μrad for Si(220), 78 μrad for Ge(111). These are equivalent to a momentum resolution at half maximum of 1.4×10^{-4} Å^{-1} and 3.1×10^{-4} Å^{-1} respectively. High resolution can thus be obtained with a double crystal diffractometer. However, the $(\Theta - \Theta_B)^{-2}$ tail of the rocking curve leads to an important background spreading over a large q range.

The use of grooved crystals instead of planar crystals does not greatly modify the width of the reflection curve but greatly reduces its wings. The n reflections which occur between the walls of one crystal changes the reflection coefficient R into R^n. This results in a very fast decrease of the tails as $(\Theta - \Theta_B)^{-2n}$; $(\Theta - \Theta_B)^{-10}$ for a 5-reflection channel cut crystal as used by Bonse and Hart [12-13].

The principle of the double crystal spectrometer is given schematically in figure 1. The first crystal, the monochromator, gives a large collimated beam whose very small horizontal

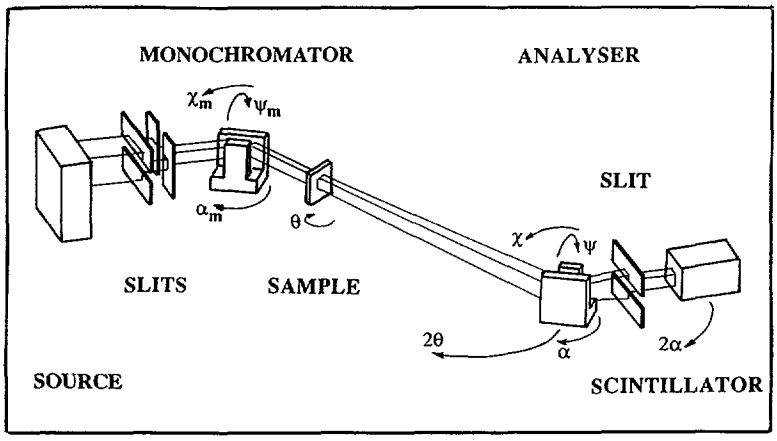

Fig. 1. — Principle of the triple axis double crystal multiple reflection spectrometer. The 3 vertical movements are around the monochromator (α_m), around the sample (θ and 2 θ), and around the analyser (α).

divergence is set by the cutting angle of the crystal [28-29]. A translational and the three rotational degrees of freedom α_m, ψ_m and χ_m are adjusted so that a broad (1 or 2 mm) beam is centered on the second axis holding the sample in a capillary for scattering in the transmission geometry. In the vertical plane, the divergence is set by the height of the source and a pair of vertical slits in front of the sample (1 to 5 mm). The collimation is typically $d\alpha \approx 80$ μrad FWHM (set by Ge 111) in the horizontal plane and $d\beta \approx 3$ mrad in the vertical plane set by the slits. The beam outgoing the sample is analysed by a second multiple reflection crystal, the analyser. There, three other rotational degrees of freedom α, ψ and χ allow a precise setting of the parallelism between the reflection planes of the monochromator and analyser crystals. The scattered light and the direct beam are measured with a scintillator associated with a photomultiplier.

The measurement of the scattering can be done either by rotating the whole detection system using the movement 2 θ around the sample axis or by rotating the analyser crystal around is own axis. The background, obtained without sample in the center of the goniometer, is the so-called « rocking-curve ». This signal has a FWHM as well as tails extending to angles larger than the reflection curves R_1 and R_2 of the two crystals according to the following convolution integral :

$$R_c(\alpha) \approx \int R_1(\alpha - \Theta) \, . \, R_2(\Theta) \, d\Theta \tag{1}$$

where α is the angle between the crystals. The rocking curve is also slightly non symmetrical. Its tails fall down as α^{-2n} when n reflections occur on monochromator and analyser crystals.

2.2 REALISATION OF THE MULTIPLE REFLECTION CAMERA. — The mechanical design is shown in figure 2. The double crystal spectrometer is built on a marble table maintaining

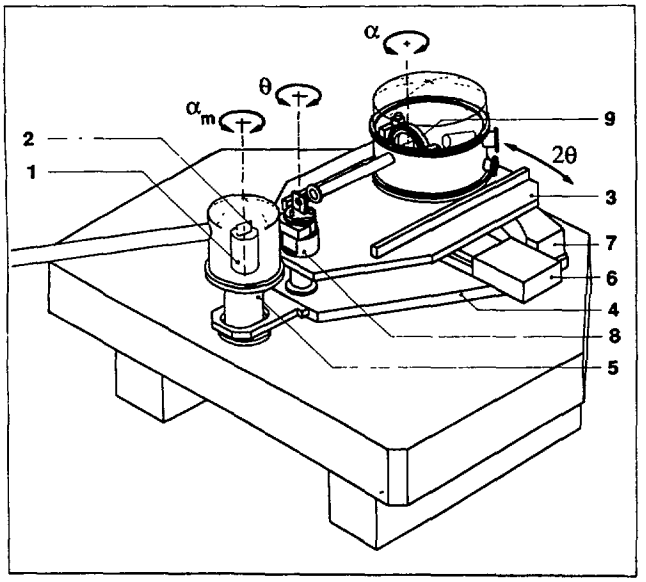

Fig. 2. — The three axis double crystal diffractometer built up in our laboratory. The first axis crosses the monochromator (manual movement), the second crosses the sample holder (θ and 2 θ rotations) and the third goes through the analyser (detector and α movement of the analyser) : 1) monochromator axis, 2) monochromator, 3) moving marble, 4) manually rotating marble, 5) monochromator holder, 6) stepping motor with linear encoder, 7) support for air cushion, 8) sample holder and 9) analyser holder.

together the three axes (monochromator, sample and analyser) with an angular stability within seconds of arc. The source (rotating anode) is not mechanically bound to the camera. The first goniometric head (n° 1) supports the monochromator (n° 2) and a thick metallic articulated protection connected to a leaded vacuum tube coming from the source. Two pairs of crossed guard slits are located just before and just after the monochromator, rotating around the crystal axis (α_m). The central part of the goniometer is a marble plateau (n° 3) rotating around the sample axis θ. The position of marmor (n° 3) can be adjusted in the center of the beam coming out of the monochromator by adjusting the underlying plate (n° 4), which moves on an air cushion.

The plateau (n° 3) rotates freely around the column (n° 5), allowing for a motion of 2 θ set by the tangential arm (n° 6) with a high precision (1 μm) optical linear encoder. The distance of the linear encoder to the rotation axis is 600 mm. There is no off axis mass balance reducing the precision of the positioning since off axis efforts are taken over by a high precision (3 μm) air cushion supporting the mass of the analysing unit and using a very flat track (n° 7) mounted on the basement (n° 4).

The sample is located on the axis of a rotating plate (n° 8). During the installation procedure, the θ and 2 θ axes have been set to be parallel within a few seconds of arc. A second conventional goniometric head (n° 9), with three rotation movements, supports the analyser crystal. The vertical rotation axis α_m of the monochromator and α of the analyser are set to be parallel within seconds of arc. The detector can be moved with a linear movement in order to follow the X-ray beam outgoing the analyser when α movement is used. Guard slits are placed in front of the analyser crystal and the detector in order to filter out as much as possible parasitic scattering. The goniometer (n° 9) and the detector can be moved towards the sample in order to adjust the sample to detector distance. The analyser crystal, guard slits as well as the detector are located in a vacuum chamber.

Figure 2 shows the multiple reflection double crystal diffractometer which was recently built in our laboratory for colloid and microemulsion studies. The source is a 18 kW rotating anode (RU300, Rigaku) with a copper target and an effective source size of 1×1 mm. The three axis goniometer has been designed and built by Microcontrôle (Evry, France) [2].

The detector and the analyser can rotate independently around the analyser axis (motion α for the analyser). They can rotate as a whole around an axis going through the sample (movement 2 θ). The sample itself can rotate around its axis (movement θ). A fourth global movement (rotation of sample + analyser + detector) around the monochromator allows us to change easily the monochromator (odd to even number of reflections, Ge to Si) or the wavelength. All movements, except the global one, are motorised with a reproducibility better than 5 μrad. For the 2 θ angle, and due to the weight of the apparatus, displacements are achieved by using a tangential arm and a linear encoder instead of a large conventional goniometer. The beam from source to monochromator and from sample to detector is maintained under vacuum to prevent both parasitic scattering and beam attenuation. The background is typically 0.3 count per second, mainly due to the dark current in the detector. The source-to-monochromator distance is about 1.2 m, sample is 15 cm further and detector 60 cm away from sample. A vertical collimating slit is located just before the monochromator and a vertical analyser slit is 52 cm away from sample, in order to allow for the deconvolution of the signal. Kα_2 line is usually filtered out by a horizontal slit placed just before the monochromator. A pair of antiscatter slits is located in front of the sample. All the data presented in the present paper have been obtained with two triple reflection Ge(111) crystals and Cu Kα radiation and a 2 θ scan, except otherwise specified.

The vertical divergence can be modified by changing the slit height. Whatever the slit conditions, the vertical divergence dβ remains much larger than the horizontal resolution dα. The two extreme vertical divergences dβ which we have used correspond to scattering

vectors dq_v of 0.009 $Å^{-1}$ and 0.1 $Å^{-1}$ dq_v can either be of the order of or much larger than the range of measured q vectors. The collimation is thus either semi-linear or linear. The angular width at half maximum of the rocking curve is equivalent to a momentum $dq_h = 3.2 \times 10^{-4}$ $Å^{-1}$

2.3 PERFORMANCES OF THE CAMERA. — The high angular resolution, obtained using a pair of Ge channel cut crystals, does not prevent the beam at the sample from having a noticeable intensity : using a 18 kW, 1 mm^2 X-ray source, we obtained a total flux exceeding 7×10^6 detected Cu Kα photons per second through the sample and the analyser, as measured with calibrated attenuators. If a very small angular fraction of the rays emitted by the source can be reflected, no spatial selection is made and the beam can be several mm high (see Tab. I). Due to the angular detection, spreading of the spatial extension of the beam at the sample does not decrease the resolution. This high resolution could only be achieved by etching the crystal at ambiant temperature with HNO_3/HF/CH_3COOH in proportions 5/3/3.

Table I. — *Specifications of our double crystal multiple reflection camera for* Ge (111) 3 *reflection crystals and* CuKα *radiation. Flux and vertical divergences depend on slit settings.*

Δq (HWHM)	1.6×10^{-4} $Å^{-1}$	
q_{min} (at 10^{-3} of maximum intensity)	4×10^{-4} $Å^{-1}$	
q_{min} (at 10^{-5} of maximum intensity)	2×10^{-3} $Å^{-1}$	
Φ (maximum flux of Rocking Curve)	1×10^6 c/s	to 7×10^6 c/s
$H \times V$ (beam size at sample position)	1×1 mm^2	2×4 mm^2
$H \times V$ (entrance solid angle)	80 μrad $\times$ 800 μrad	80 μrad $\times$ 3 mrad
$H \times V$ (analysis solid angle)	80 μrad $\times$ 2 mrad	80 μrad $\times$ 16 mrad

The rocking curve of the empty camera (without sample) obtained in our laboratory is plotted in figure 3. The usual two experimental methods have been used. When a rotation of angle α is performed around the analyser the direct beam always irradiates the analyser crystal. Scanning angle 2 θ around the sample displaces the analyser slits, the analyser and the detector all together. With the triple reflection Ge crystals we use, the two rotation methods give nearly identical results.

Only a small difference is observed near $\alpha = 2\,\theta = 1$ mrad, certainly due to the scattering by the analyser slit. However the slits cannot be removed since they prevent the direct beam from falling out of the analyser crystal channel for non zero 2 θ. Rotating the second crystal around the α axis is safer because the same point of the crystal surface is used, avoiding errors due to surface inhomogeneities (Deutsch, personal communication). The rocking curves obtained by these methods are compared to the theoretical triple reflection profile. The difference in width can be explained by a mosaicity of 10 μrad (2″ of arc) of the Ge material over the effectively used scattering volume of the monochromator material. The rocking curves show a decrease of the tails by several orders of magnitude and a q^{-6} decrease is observed near a scattering angle of 100 μrad.

A quality criterion of the camera for a given scattering momentum q is the rejection rate $R(q)$, that is the ratio of the remaining background for this q value relative to the maximum intensity of the rocking curve. Rejection ratios $R = 10^{-5}$ and $R = 10^{-4}$ are obtained for deviation angles 2 Θ of 1 mrad and 0.1 mrad respectively. For angles larger than 10 mrad or distances $D^* = 2\,\pi/q$ smaller than 300 Å, the rocking curve is limited by the detector background and leads to a rejection ratio $R \approx 5 \times 10^{-8}$ These can be compared to the performance of our GDPA 30 camera : a Guinier-Mering type camera manufactured by the

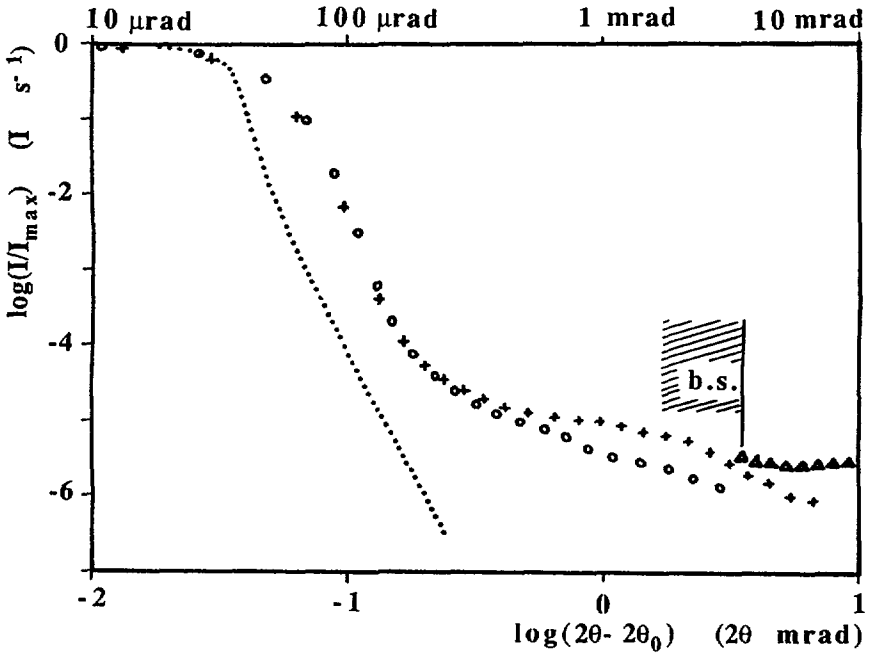

Fig. 3. — Rocking curves obtained by rotating either α (O) or 2 θ (+) and theoretical rocking curve (...) for 2 perfect 3 reflections Ge 111 grooved crystals. The maximum value is normalized to unity. On the same scale is also indicated the background scattering measured at the beamstop (BS) edge of our CGR camera (Δ). In the latter, the beam focusing occurs with a bent and asymmetrically cut (6°) Ge crystal.

Compagnie Générale Radiologique at Issy-les-Moulineaux (France) in 1970. Here the minimum useful angle is limited by the beam-stop size in front of the detector plane. This size is given by the tail of the direct beam, i.e. the beamstop extends to an angle 2 Θ where the parasitic scattering is of the order of magnitude of the scattering coming from the sample. Triple reflection Ge crystals yield good rejection factors up to particle sizes D^* a few hundred nanometers. A comparison of our camera with the pinhole collimation SANS D11 camera at ILL and the double crystal S21 camera at ILL has been performed by Lesieur *et al.* [30].

3. Data analysis method.

The goal of scattering experiments is to measure the differential cross section density $d\Sigma/d\Omega$ of a sample or of a series of samples. Let us consider a sample of thickness t, made of n uncorrelated particles, having individual cross sections σ. Without multiple scattering one has experimentally access to the quantity :

$$\frac{d\Sigma'}{d\Omega} = t\frac{d\Sigma}{d\Omega} = tI_a(\Omega) = tn\frac{d\sigma}{d\Omega} \tag{2}$$

where $d\Sigma'$ is the probability for a given photon to be scattered in $d\Omega$ when crossing the sample and has no unit, $d\Sigma'/d\Omega$ can be expressed in rad^{-2} and $d\sigma/d\Omega$ in $cm^2\,rad^{-2}$ The quantity $d\Sigma/d\Omega$ is also called the absolute intensity $I_a(\Omega)$, is expressed in $cm^{-1}\,rad^{-2}$ One uses more often as a short cut cm^{-1} for $I_a(\Omega)$ instead of $cm^{-1}\,rad^{-2}$

3.1 THE SMEARING PROBLEM. — In a real experiment, the incident beam is not parallel and the scattered light is not measured within an infinitesimal solid angle. One does not measure directly the differential cross section density $d\Sigma/d\Omega$ but an average of $d\Sigma/d\Omega$ over the angular divergences of both the incident and scattered beams. With a multiple reflection camera the angular divergence of the incident beam is defined in the horizontal plane by the acceptance angle of the monochromator. Since the radiation emitted by a conventional source is very broad, the angular distribution of the inensity for a given wavelength is proportional to the reflection coefficient $R_{mono}(\alpha)$ of the crystal, where α is the output angle of the X-rays. In the vertical plane, the divergence of the beam is defined by the height of the source and that of the collimating slit located near the monochromator. After Lesieur the angular distribution of the direct beam intensity after the monochromator can thus be factorized as follows [31] :

$$\left(\frac{dI}{d\Omega}\right)(\Omega_0) = \left(\frac{dI}{d\Omega}\right)(\alpha_0, \beta_0) = I_0 \cdot f_{mono}(\alpha_0) \cdot g(\beta_0) \tag{3}$$

$f_{mono}(\alpha)$ is proportional to the reflection coefficient of the crystal. The function $g(\beta)$ is defined by the vertical dimensions of the source and of the collimating slit. They will be normalized later, thus defining the coefficient I_0.

Usually the function $g(y)$ has the shape of a trapezium. Figure 4 shows an experimental vertical profile of the direct beam. It has been measured in the plane of the analyser slit. One clearly sees the central plateau and the symmetric shadowed zones on both sides with a linear decrease of flux with vertical position. Position has been converted to angle seen from the sample. In order to obtain reliable desmeared spectra, such profiles are systematically measured with an Image Plate detector system described in [32].

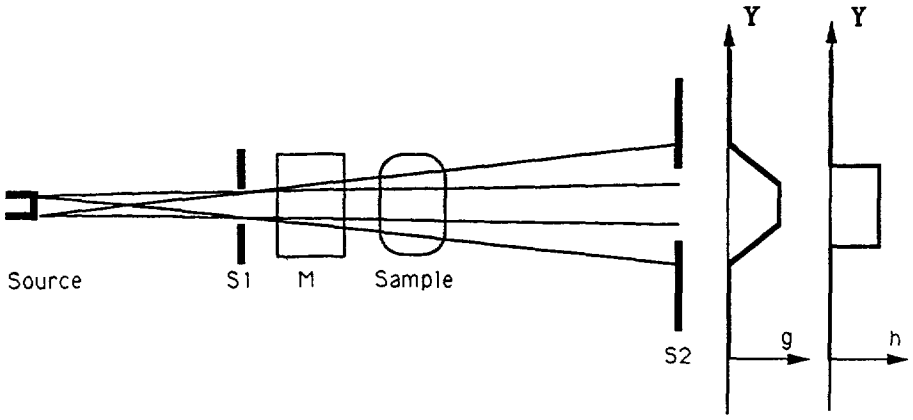

Fig. 4. — Vertical plane cut of a Bonse-Hart camera designed for a conventional source. S1 is the collimating slit and S2 the analyser slit, M represents the monochromator. The typical intensity profile of the beam $g(y)$ in the plane of the analyser slit and the transmission step function $h(y)$ of the analyser slit are shown on the right.

3.2 ROCKING CURVE WITHOUT SAMPLE. — The detection system is composed of a slit which limits both the beam and the scattered rays in the vertical direction, an analyser crystal and a detector. The response function $E(\Omega_1)$ of the whole can be factorized as follows :

$$E(\Omega_1) = E(\alpha_1, \beta_1) = f_{ana}(\alpha_1) \cdot h(\beta_1) \tag{4}$$

$f_{ana}(\alpha_1)$ is proportional to the reflection curve of the analyser crystal and $h(\beta_1)$ is the step function defined by the analyser slit height. The intensity measured without sample or the « rocking curve » is the intensity of the direct beam $(dI/d\Omega)(\Omega)$ falling on the detection system multiplied by its efficiency $E(\Omega)$ and averaged over the solid angle Ω. If the analyser crystal is rotated by an angle α one obtains :

$$I_{beam}(\alpha) = \int d\Omega_0 \left(\frac{dI}{d\Omega} \right) (\Omega_0) \cdot E(\Omega_0 - \alpha) \tag{5}$$

or in a more explicit way :

$$I_{beam}(\alpha) = I_0 \int d\alpha_0 f_{mono}(\alpha_0) f_{ana}(\alpha_0 - \alpha) \cdot \int d\beta_0 g(\beta_0) h(\beta_0) . \tag{6}$$

The integral over angle α represents the angular profile $R_c(\alpha)$ of the rocking curve :

$$R_c(\alpha) = \int d\alpha_0 f_{mono}(\alpha_0) \cdot f_{ana}(\alpha_0 - \alpha) . \tag{7}$$

The second integral in equation (6) is a constant. Anticipating to later results, we shall call it $V(0)$ where $V(\beta)$ is given by :

$$V(\beta) = \int d\beta_0 g(\beta_0) h(\beta_0 + \beta) . \tag{8}$$

We shall normalize the functions $R_c(\alpha)$, $g(\beta)$ et $h(\beta)$ so that :

$$V(0) = 1 \quad \text{and} \quad \int_{-\infty}^{+\infty} R_c(\alpha) \, d\alpha = 1 . \tag{9}$$

This leads to the simple relation :

$$I_{beam}(\alpha) = I_0 \cdot R_c(\alpha) . \tag{10}$$

We now see that the constant I_0 is equal to the angular integral of the experimental rocking curve. If the analyser slit truncates the direct beam, the condition $V(0) = 1$ means that I_0 is the angular integral of this fraction of the direct beam which goes through the analyser slit. The measured intensity $I_{beam}(\alpha)$ is expressed in counts.s^{-1}, $R_c(\alpha)$ is in rad^{-1} and I_0 is in rad.counts.s^{-1}. With a maximum intensity of 3×10^6 counts.s^{-1} and an angular width near 100 μrad, I_0 is about 300 rad.counts.s^{-1}

$$I_0 = \int I_{beam}(\alpha) \, d\alpha . \tag{11}$$

Fig. 5. — Experimental vertical profiles of the direct beam in the plane of the analyser slit measured with phosphorescent screens and scanner. Such profiles are determined by the vertical sizes of the source (1 mm) and of the collimating slit (4 mm).

3.3 INTENSITY SCATTERED BY THE SAMPLE. — One ray with incident direction $\Omega_0 = (\alpha_0, \beta_0)$, and intensity $(dI/d\Omega) \cdot d\Omega_0$ after transmission through the sample, gives rise to a scattered intensity $(dI/d\Omega)_{\Omega=\Omega_0}\ d\Omega_0 \cdot (d\Sigma/d\Omega)_{\Omega=\Omega_1-\Omega_0}$ per unit solid angle $d\Omega_1$ in direction Ω_1. Transmitted later by the analyser tilted by an angle α and counted by the detector with global efficiency $E(\Omega_1 - \alpha)$, the scattered and measured intensity is obtained by integration over the solid angles Ω_0 and Ω_1.

$$I_m(\alpha) = \int d\Omega_0 \int d\Omega_1 \left(\frac{d\Sigma'}{d\Omega} \right) (\Omega_1 - \Omega_0) \cdot \left(\frac{dI}{d\Omega} \right) (\Omega_0) \cdot E(\Omega_1 - \alpha) . \tag{12}$$

If we use the previous expressions of $dI/d\Omega$ and $E(\Omega)$ it comes :

$$I_m(\alpha) = I_0 \int d\Omega_1 \left(\frac{d\Sigma'}{d\Omega} \right) (\Omega_1) \cdot \int d\Omega_0 f_{mono}(\alpha_0) f_{ana}(\alpha_0 + \alpha_1 - \alpha) g(\beta_0) h(\beta_0 + \beta_1) \tag{13}$$

or after some rearrangement using equations (7) and (8) :

$$I_m(\alpha) = I_0 \int d\Omega_1 \left(\frac{d\Sigma'}{d\Omega} \right) (\Omega_1) \cdot \int d\Omega_0 f_{mono}(\alpha_0) f_{ana}(\alpha_0 + \alpha_1 - \alpha) g(\beta_0) h(\beta_0 + \beta_1) . \tag{14}$$

For an isotropic sample $d\Sigma'/d\Omega$ is only a function of the scattering angle $2\theta = (\alpha_1^2 + \beta_1^2)^{1/2}$ If, as is usually the case, the width of the scattered intensity $d\Sigma'/d\Omega(2\Theta)$ is much larger than the width of the rocking curve $R_c(\alpha)$, the convolution in the horizontal direction (along angle α, where the resolution is high) can be suppressed. One thus obtains the expression characteristic for smearing due to linear or quasi-linear collimation :

$$I_m(\alpha) = I_0 \int_{-\infty}^{+\infty} d\beta_1 \left(\frac{d\Sigma'}{d\Omega} \right) (\sqrt{\alpha^2 + \beta_1^2}) \cdot V(\beta_1) . \tag{15}$$

Here the rocking curve $R_c(\alpha)$ is normalized according to previous condition (12). $(\alpha^2 + \beta_1^2)^{1/2}$ represents the effective scattering angle. Due to the additivity of α^2 and β_1^2 it is much simpler to write I_m and $d\Sigma/d\Omega$ as functions of α^2. The following equivalent expression, presented as a true convolution product yields an inversion formula giving $d\Sigma'/d\Omega(\alpha)$ when $I_m(\alpha)$ is known. If we replace $d\Sigma'/d\Omega(\alpha)$ by $I_a(\alpha)$, we get :

$$I_m(\alpha^2) = tI_0 \int_0^{\infty} du\, I_a(\alpha^2 + u) \cdot G(u),\ G(u) = \frac{V(\sqrt{u}) + V(-\sqrt{u})}{2\sqrt{u}} \tag{16}$$

3.4 SOLUTIONS FOR THE DESMEARING PROCEDURE. — Many papers have proposed solutions to the linear collimation smearing problem. The problem was already known in the 50's as well as the solution for the case of an infinite slit [11].

When the vertical divergence is so large that the quasi-linear collimation becomes an infinite slit collimation, then the function $V(\beta)$ can be set equal to 1 and the apparatus function is equal to $G(u) = 1/\sqrt{u}$. Invertion of smearing equation can be performed analytically. Following Guinier and Fournet [11] we have :

$$I_a(\alpha^2) = \frac{1}{t} \left(\frac{d\Sigma'}{d\Omega} \right) (\alpha^2) = \frac{1}{\pi t I_0} \frac{d}{d - \alpha^2} \int_0^{\infty} du\, I_m(\alpha^2 + u) \cdot \frac{1}{\sqrt{u}} . \tag{17}$$

Apart from the leading constant $1/(\pi t I_0)$ this equation tells us that, in order to desmear the experimental spectrum, one has to resmear with the same smearing function $1/\sqrt{u}$ and then take the derivative (relative to coordinate $-\alpha^2$). Note that both smeared and unsmeared intensities are expressed as functions of squared angles α^2.

In the finite slit case, the main problem is to find the inverse of the smearing function $G(u)$. An early solution has been proposed by Kratky [33] when the weighing function has a Gaussian shape. Numerical tests of the deconvolution have been performed by Schmidt [34] for Gaussian weighing functions.

An iterative method has been proposed by Lake [35] to desmear experimental spectra. In fact it smears a hypothetical desmeared curve, compares the resulting curve with the experimental one and adjusts the desmeared curve to get a good fit between the calculated smeared curve and the experimental spectrum. Tests of Lake's method have been performed by Schmidt [34]. An advantage of this method lies in the fact that different smearings (due to slit height, slit width or radiation bandwith) can be corrected at once. However, convergence has not been proved and is not always good [36].

Deutsch and Luban [36-39], Schmidt and Ferodov [40], have developed methods to solve the problem as posed by Kratky. The case of a Gaussian weighing function is often considered but more realistic cases of rectangular or trapezoidal distributions of intensity of the direct beam in the detector plane are developed by Luban [38] and Schmidt [40], respectively.

A least squares method has been proposed by Glatter [41-42]. The unsmeared intensity or its Fourier transform (the Patterson function) is expanded on a basis of appropriate functions : $I(q) = \Sigma C_n \cdot I_n(q)$. It is then smeared, compared to the experimental spectrum and the coefficients C_n are determined by a least square procedure. This method needs a maximum particule size and is not well suited to interacting particules. Efforts are currently being made to remove this condition [43].

3.5 AN ALGEBRAIC SOLUTION. — A formulation has been given by Strobl [44] in order to develop an efficient method for desmearing spectra from a Kratky camera. It has recently been adapted and used by Lesieur and Zemb for multiple crystal cameras [30-31]. Strobl introduced a function G^* defined by :

$$\int_{-\infty}^{\infty} dv\, G(v) \cdot G^*(u - v) = Y(u) = \begin{cases} 0 \text{ if } u < 0 \\ 1 \text{ if } u > 0 \end{cases} \tag{18}$$

where $Y(u)$ is the Heavyside function. The analytical solution $G^*(u) = 1/(\pi\sqrt{u})$ is valid for small u. For larger u, $G^*(u)$ can be determined recursively from small to large values of u. The smearing of $I_m(\alpha)$ with function G^* leads to the primitive (*versus* $-\alpha^2$) of the absolute intensity $I_a(\alpha)$. Taking then the derivative one gets the following simple formula [31] :

$$I_a(\alpha^2) = \frac{1}{t}\left(\frac{d\Sigma'}{d\Omega}\right)(\alpha^2) = \frac{1}{tI_0}\frac{d}{d(-\alpha^2)}\int_0^{\infty} du\, I_m(\alpha^2 + u) \cdot G^*(u) . \tag{19}$$

If one determines the constant I_0, i.e. if one measures the direct beam intensity (usually through a calibrated attenuator to prevent saturation of the detector) and the scattered beam with exactly the same slit heights, then desmeared spectra on the absolute scale in $cm^{-1} \cdot rad^{-2}$ can be obtained. Since I_0 is the area of the direct beam transmitted through the sample, the correction due the transmission factor of the sample is performed in the same step.

Let us sum up the procedure and give a simple recipe to desmear on an absolute scale.

Starting with an experimental spectrum $I(\Theta)$ in counts.s^{-1}, integrate the central region corresponding to the direct beam transmitted by the sample. I_0 in rad.counts.s^{-1} is obtained. Then divide $I(\Theta)$ by this area I_0 and also by the thickness t of the sample. This gives a new smeared intensity in cm^{-1} rad^{-1}. Now desmear it with a $G^*(\beta^2)$ function in rad^{-1} and get the desmeared intensity on the absolute scale in $cm^{-1}.rad^{-2}$ We finally insist upon the use of angles in radians (never use another unit nor q in $Å^{-1}$) so that as few constants as possible are introduced.

3.6 DESMEARED APPARATUS FUNCTION ON AN ABSOLUTE SCALE. — Smearing and desmearing equations are linear transformations. Thus it is meaningful to desmear the rocking curve recorded with the empty camera. Several rocking curves corresponding to different vertical apertures have been plotted in figures 6a and 6b. On a linear scale we can see that the width of the rocking curve does not vary with the vertical divergence (Fig. 6a). Figure 6b shows that rocking curves recorded with different beam powers and different vertical beam divergences lead to nearly the same apparatus function after desmearing and scaling. For the latter operation, a standard sample thickness of 0.1 cm was used. A small deviation is observed at large momentum : rocking curves measured with a large divergence, and thus a high beam intensity are less sensitive to the detector background. The region below the curves shows in figure 6b is accessible only after subtraction of a high background. These curves can be considered as a lower limit to the measurement of a real $I(q)$ spectrum.

They can be compared to a theoretical calculation of $I(q)$ before studying a new sample. For comparison to scattering by spheres, the envelope of $P_R(q)$ curves for spheres of radius

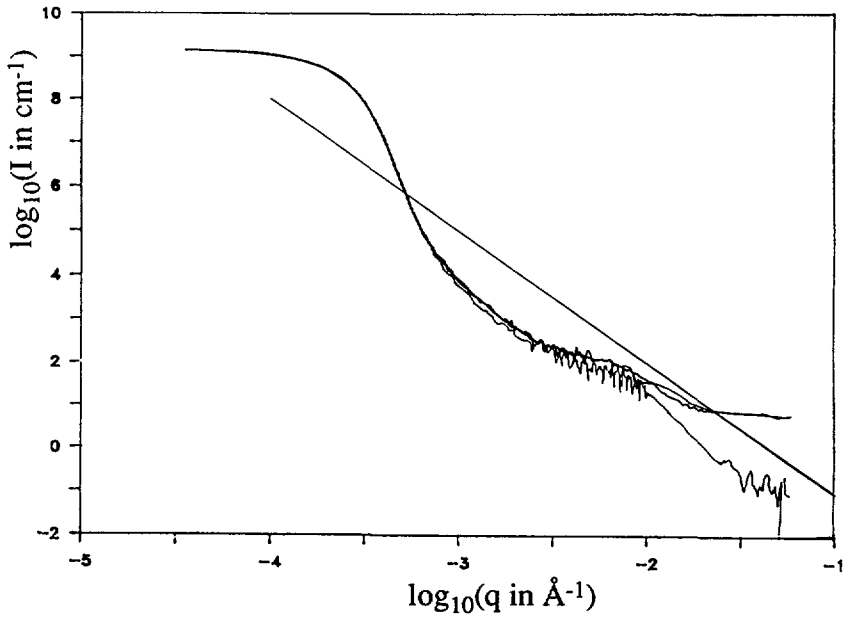

Fig. 6. — Log-log plot of the desmeared rocking curves on the absolute scale obtained with 2 identical 3 reflection Ge 111 channel cut crystals and different vertical divergences. A better sensitivity can be observed at large q with a larger vertical divergence. The straight line, whose slope is -3, represents the envelope of $P_R(q)$ curves for spheres of radius R when R is varied. It is also equal to $P_R(q)$ for $q.R = 2.46$. The contrast of spheres relative to solvent is $\Delta B = 10^{-5}$ Å/Å^3 i.e. $\Delta\rho \approx 0.3$ e/Å^3 or the electron density of water for SAXS. The volume fraction is 0.1 %.

R, when R is varied, has been drawn. It is a straight line whose slope is -3. The $P_R(q)$ curves are tangent to this line for $q \cdot R = 2.46$. The volume fraction is set to 0.1 % and the contrast of spheres relative to solvent is $\Delta B = 10^{-5}$ Å/Å^3 or $\Delta\rho = 0.3$ e/Å^3 i.e. the effective electron density of water for SAXS.

4. Experimental examples.

4.1 RESOLUTION LIMIT : SCATTERING FROM THE RAT TAIL COLLAGEN FIBERS. — In order to compare the possibilities of a focusing camera and a multiple crystal camera on a typical colloidal sample, we decided to measure the same sample made of a bundle of strained aligned wet rat tail collagen fibers [45] with a focusing camera and our triple axis laboratory setup. The best focusing camera available in our neighbourhood is the double monochromator setup D22 in permanent use at L.U.R.E. (Orsay, France) developed by C. Williams. The characteristic flux at the time of the measurement was 5×10^7 photons.s^{-1} for a 10 keV energy. This value was estimated by using the scattering given by a 1.5 mm thick water sample in a given solid angle. The 2 mm wide beam-stop is located near the detector 1.5 m after the sample. Its size is imposed by the divergence of the beam, in order to obtain a total flux of the order of 100-300 photons.s^{-1} in the detector, but outside the beam-stop. The beam-stop size limitation is given by the defects of the two Ge crystals used as monochromators.

Figure 7 compares the results obtained with a 5 h scan of the first Bragg peak obtained in the laboratory using the multiple crystal method. With a linear detector on a storage ring, twenty orders of reflection are easily seen with a gas detector ; however, the first few orders are superimposed to a big « tail » of parasitic scattering. The width of each peak is the same on all orders (2×10^{-3} Å^{-1}) and is slightly larger than the size of the beam in the detector plane, due to the resolution of the electronics (300 μm FWHM). Three peaks can be accurately scanned during a 24 h experiment in the laboratory : these peaks have the same width as the empty camera rocking curve (3×10^{-4} Å^{-1} FWHM, or 2 μm Bragg periodicity in real space !). The q-independent resolution of the multiple reflection camera is therefore of

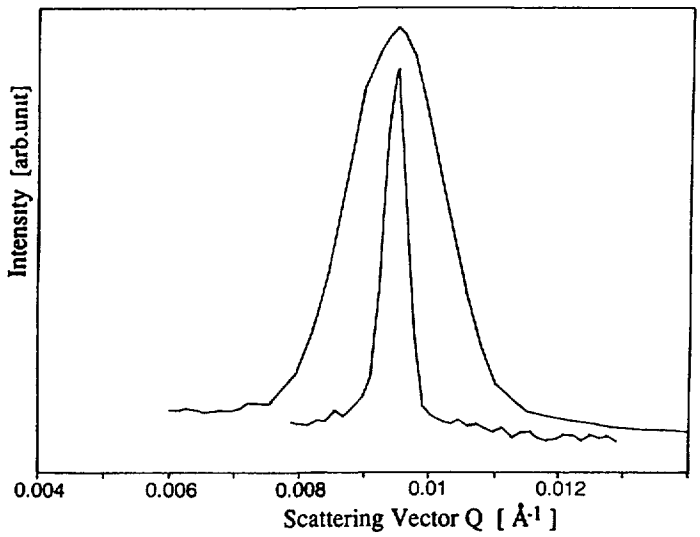

Fig. 7. — First peak of the X-ray diffraction spectrum from the rat tail collagen fibers obtained on the Bonse-Hart camera (lower curve, scanning time 5 h) compared to that obtained with D22 camera at LURE (upper curve, 1 h exposure).

the order of 1 μm, Bragg spacing. The spatial extent of the monocrystalline arrangement of the rat tail collagen is larger than our resolution. Hence, the same wet collagen reflections used to calibrate the neutron D11 camera at Institut Laue-Langevin are a very handy sample for checking resolution in USAXS.

4.2 EFFECT OF SLIT HEIGHT : SCATTERING FROM PACKED SILICA SPHERES. — In order to check our apparatus as well as the deconvolution procedure, spectra from a unique sample with different experimental conditions were recorded and desmeared. The sample is a silica gel in a solid state obtained by aggregation and drying of monodispersed silica spheres in solution (thickness = 0.07 cm). The radius of these spheres as determined by the oscillations seen in the X-ray scattering pattern is about 1 500 Å. Both the monochromator and the analyser slits have been varied by modifying either the direct beam profile or the analyser slit function. The slit heights as well as the small and large bases of the trapezoidal vertical profile of the direct beam in the plane of the analyser slit have been measured as exposed previously and the results are given in table II.

Table II. — *Experimental collimation conditions, momentum δq_v equivalent to the half width of smearing function $V(\beta)$ and limit slope in the Porod region as used to test the desmearing procedure.*

Parameter for spectrum	A	B	C	D	E	F
Analyser Slit (mm)	24	24	4	1	1	0.5
Collimation Slit (mm)	4	—	2	1	1	1
Small Base (mm)	6.2	5.3	1.8	0.6	0.5	0.5
Great Base (mm)	8.4	7.1	3.9	2.7	2.9	2.9
Limit slope :						
— smeared	− 3.05	− 3.0	− 3.42	− 3.75	− 3.75	− 3.8
— unsmeared	− 4.0	− 4.0	− 3.9	− 4.0	− 4.0	− 4.0
δq_v	0.11	0.12	0.027	0.01	0.01	0.0086

This sample, provided by Dr. Joanicot, exhibits a large contrast (silica relative to air). At constant volume fraction, the scattered intensity is proportional to the volume of the particles, that is, to the third power of the radius. This largely favours spheres with a 1 500 Å radius relative to smaller ones. These reasons together with the fact that no multiple scattering has been observed, supported our choice of this sample as a real deconvolution test sample.

The experimental spectra on a logarithmic scale are given in figure 8a. All the curves have been normalized to the maximum of the first peak. Near the first maximum the different curves can hardly be differenciated. In fact the vertical divergence converted in momentum units (see Tab. II) is always much larger than the position q_{max} of the maximum of the peak. The collimation in this q range is always equivalent to that of an infinite slit.

The desmeared curves (according to the procedure previously described) are displayed in figure 8b. The spectra are presented exactly as they appear at the end of the procedure and no factor has been introduced in order to rescale the maxima of the first peak. A systematic spacing of 0.5 log unit has been introduced to prevent a superposition of the curves. This clearly shows that desmearing and scaling to absolute intensity work very well in practical cases. After desmearing, the first peak is much more narrow and characteristic of strongly interacting spheres. Relative to the peak position observed before desmearing, it is also

shifted towards larger q values : smearing a peak enhances the intensity at a momentum below q_{max} but not at a momentum above q_{max}, i.e. smearing shifts a peak to lower q values.

The absolute intensity about 10^6 cm^{-1} is orders of magnitude above the usual range for micelles (about 10^{-2} to 1 cm^{-1}) : a factor of 100 for the radius leads to an increase by a factor of 10^6 for the intensity further enhanced by the high contrast. Large particles are very intense scatterers. The reproducibility and the quality of the spectra clearly show that the multiple crystal camera is very well suited to study large objects for which light scattering should present multiple scattering.

For large q values the curves present many oscillations of the form factor for sphere. The limit slope in the Porod region varies from – 3 to – 4 for the experimental smeared spectra depending on the vertical slit settings (see also Tab. II). That is, when one slit height increases, the collimation varies at a given but large q from a punctual to a linear one. The intermediate curve with a slope of – 3.5 shows that collimation can continuously vary from punctual to linear.

After desmearing the limit slope in the Porod region is always very close to – 4 as is shown in figure 8b. The oscillations of the form factor for spheres are nicely superposed. A well defined limit can be found for q^4 I (q) giving access to the specific interface area without use of the invariant. This has been recently used to determine the specific area of emulsified oil droplets [30].

4.3 INTERACTING SPHERICAL COLLOIDAL PARTICLES : FLUORINATED LATEXES. — Let us now turn towards another class of problems in the physics of colloids : the knowledge of the pair interaction potential between spherical colloids is crucial in order to understand the

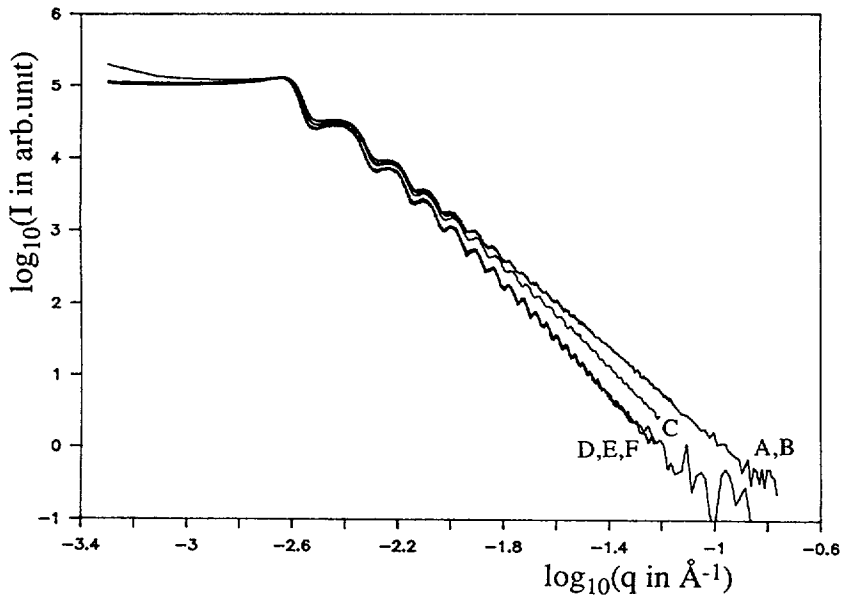

a)

Fig. 8. — Spectra from a silica gel in the solid state are presented on a log-log plot. a) All the experimental (smeared) curves have been normalized to the maximum of the first peak. More than ten oscillations of the form factor for the spheres can be observed. The Porod region shows slopes between – 3 and – 4. b) After desmearing the first peak and the oscillations are more pronounced. The upper curve is in cm^{-1}. An offset of 0.5 log unit between successive spectra has been introduced for clarity. The high q limit always shows a – 4 slope.

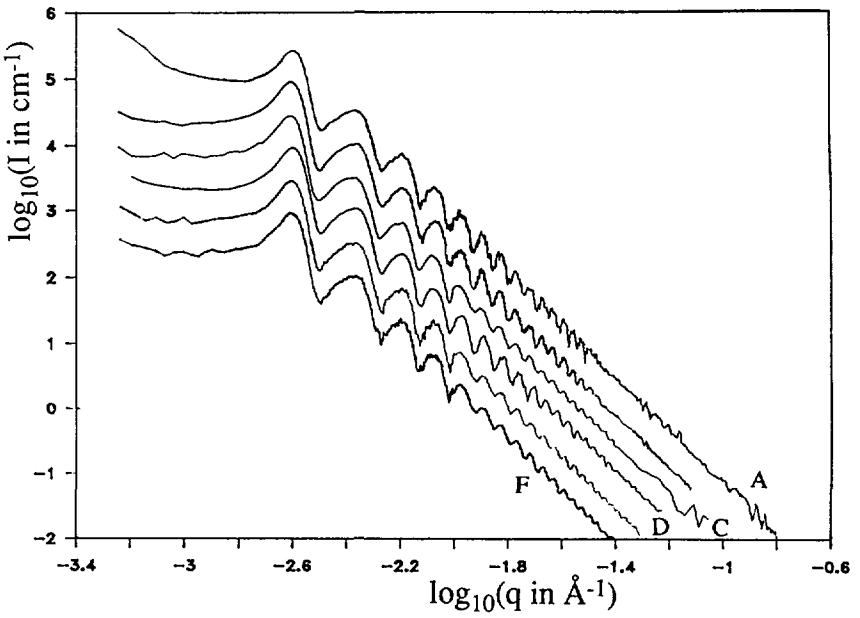

b)

Fig. 8 *(continued).*

physics of interfaces at the nanometric scale. The first quantitative self-consistent approach has been made using the so-called « rescaled mean spherical approach » (RMSA) by Hansen and Hayter [46-47], and applied to micelles. The analytic expression of the potential is supposed to be known and is the screened electrostatic potential : simultaneous determination of the form factor $P(q)$, the scattering of a single colloid, and the interparticle structure factor $S(q)$ allow a direct measure of the net surface charge measured at the hard sphere radius as well as the mass of the particle. This method is now routinely used to analyse the interaction in colloidal systems for small particles of radius less than 100 Å [48-49].

By extending the q-range to lower angles, there is a possibility of determining the energy of contact of two large spherical colloidal particles, without any extrapolation towards infinite dilution. We choose to show this on a concentrated solution of fluorinated latex particles : the radius is easy to determine using the oscillations obtained on the deconvoluted spectra at large angles : the radius of the latex spheres used is 800 Å. These fluorinated latex solutions kindly provided by Piazza are well characterized [50-51] : the density is well known and equal to 2.1 g/cm^3 ; the mass fraction (and thus volume fraction) can be easily determined by evaporation of the solvent and weighing. Data have been obtained at 5 % and 10 % volume fraction. Figure 9 represents a desmeared spectrum recorded for a volume fraction of latex in water $\varphi = 10$ %. The invariant Q^* has been calculated for these spectra according to the following equation :

$$Q^* = \int_0^\infty q^2 I_a(q)\, dq = 2\,\pi^2 (\Delta B)^2\, \varphi\,(1-\varphi)\,. \tag{20}$$

The comparison of the invariants obtained from X-ray scattering *via* the second term of equation (20) and that obtained from the chemical characterization of the sample agree well ($Q^* = 95 \times 10^{-12}$ Å^{-4}). The scattered intensity $I(q)$ was calculated using the Hayter-Penfold method [47] by using only the net surface charge as a free parameter. A very good fit is obtained on the absolute scale for a charge of 9×10^{-17} C, leading to a surface charge of

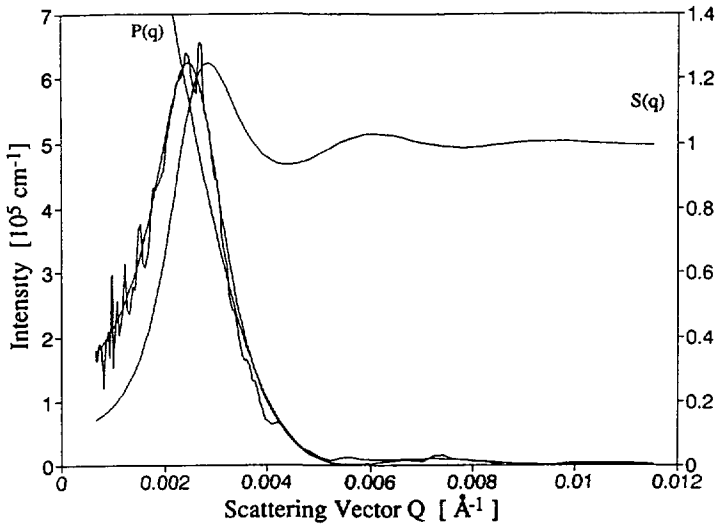

Fig. 9. — Interaction peak of a solution of perfluorinated latex spheres after desmearing on an absolute scale. 10 % volume fraction, 800 Å radius. A fit of the experimental spectrum by $I(q) = P(q) \cdot S(q)$ is shown together with the $P(q)$ and $S(q)$ factors.

0.1 μC/cm^2, which is a quite typical value. The $P(q)$ and the $S(q)$ factors have also been drawn. Repulsions between the spheres lead to a quite small value of $S(q)$ at $q = 0$. This experiment shows that USAXS using a multiple crystal setup allows the determination of interparticle scattering with particles as large as 1 000 Å, when desmeared data are available at $q \approx 10^{-3}$ Å^{-1}

4.4 SCATTERING BY POROUS GRAPHITE. — In order to characterize the porosity of crosslinked or highly connected dry materials such as catalysts, cross-linked polymer resins or porous coal, a careful determination of the exponent β in the scattering of the form $I(q) = q^{-\beta}$ is needed. Here, the problem is to discard instrumental broadening, deformation due to large count-rate contrasts in position sensitive detectors or multiple scattering effects. The scattered intensity may be large enough : the multiple reflection Bonse-Hart setup is here the most reliable experimental technique to obtain an artefact-free scattering curve extending over two decades at least in the q-direction. For mass fractals, the exponent β is between 1 and 3 ; for surface fractals, the exponent is between 3 and 5 [52-53]. When the exponent is exactly 4, a direct determination of the surface-to-volume ratio is possible (Porod law) if the scattering measurements are made on absolute scale and if the electron density contrast is known. If a surface layer of constant thickness is adsorbed at the surface, such as for example a surfactant layer, the asymptotic limiting law is the sum of q^{-4} and a q^{-2} terms, which complicates the analysis.

As an example of the use of a multiple crystal camera, we choose to measure the low end of the scattering of porous coal kindly provided by Pr. Schmidt. A debated question is whether a fractal structure is responsible for the deviation observed towards the Porod law with porous graphite powder [54-55]. We recorded the spectra for different slit heights, as we did with the silica sphere samples. The spectra are very smooth and no structure is present. Before desmearing, the slope varies from -2.7 to -3.6, after desmearing a slope of -3.7 ± 0.1 is obtained with our camera (see Fig. 10a). This measured slope is the same as that obtained by Schmidt by using other methods. The absence of structures and the limiting slope away from

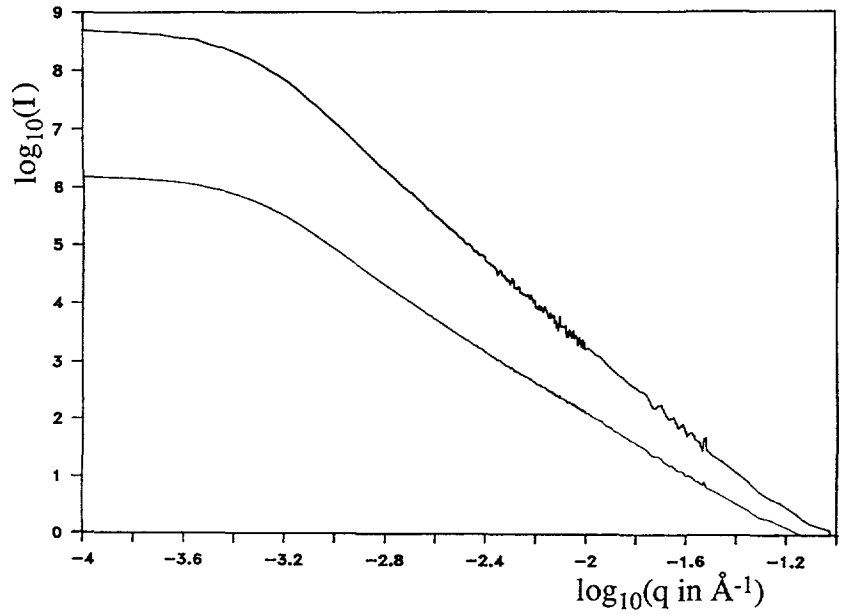

a)

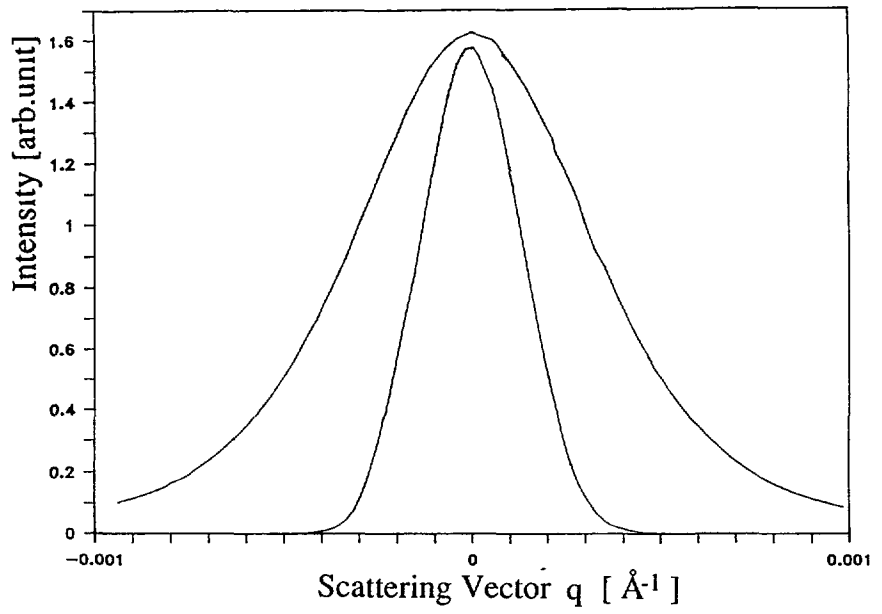

b)

Fig. 10. — a) Spectrum from porous graphite before and after desmearing on a log-log plot. Before deconvolution (lower curve, I in counts/s) a -2.7 slope is observed. After deconvolution (upper curve, I in arb. unit) a -3.7 slope is obtained. b) Linear plot of the direct beam. The important broadening indicates the presence of multiple scattering or refraction by the graphite crystallites.

– 4 are generally presented as arguments in favour of a fractal structure. With our sample, whose thickness is about 0.05 cm, we observed that multiple X-ray scattering is present at low q values as shown in figure 10b. The scattering is so intense that a very broadened beam but not the direct beam is observed after the sample. It may also be due to refraction of the direct beam through the crystallites of graphite. In this case, the – 3.7 slope is undoubtedly due to the fractal geometry of porous graphite. A possible effect of the thickness of the sample is however difficult to test due to the difficulty in obtaining very thin homogeneous samples. For this sample the background of the camera could not be subtracted due to the broadening of the direct beam but it was much lower than the scattering by the sample. When scattering is very intense a procedure similar to that of Dwiggins might be used for background subtraction [56].

4.5 SWOLLEN LAMELLAR PHASES OF FLUOROCARBON SURFACTANTS. — A few surfactants showing low solubilities in water can form spontaneous swollen liquid crystals at high dilution : binary surfactant-water mixtures show fluid birefringent phases with only a few percent weight surfactant. The microscopic periodicity between repulsive bilayers in these solutions is of the order of 1 000 Å. Chittofrati [57] and Dubois [58] have shown that some perfluoropolyethers (PFPE) show this behaviour in water. The repulsive force responsible for this swelling is the screened electrostatic force and the swelling is limited by an order-disorder transition towards a disordered connected lamellar phase [59].

Using neutron scattering, the Bragg peaks indexed 1-2-3 are easily measured with an exposure time of a few minutes in the q-range 10^{-2} Å^{-1} to 10^{-3} Å^{-1} allowing precise determination of the spacing. However, up to now, Bragg peak width could nether be measured in the electrostatic repulsion case on swollen lamellar phases by using neutron scattering because the powder ring width is limited by the source size (collimation). We therefore measured the Bragg peak widths on PFPE solutions provided by Montefluos Spa. A spectrum from a 0.5 % w/w solution of PFPE in water at room temperature is shown in

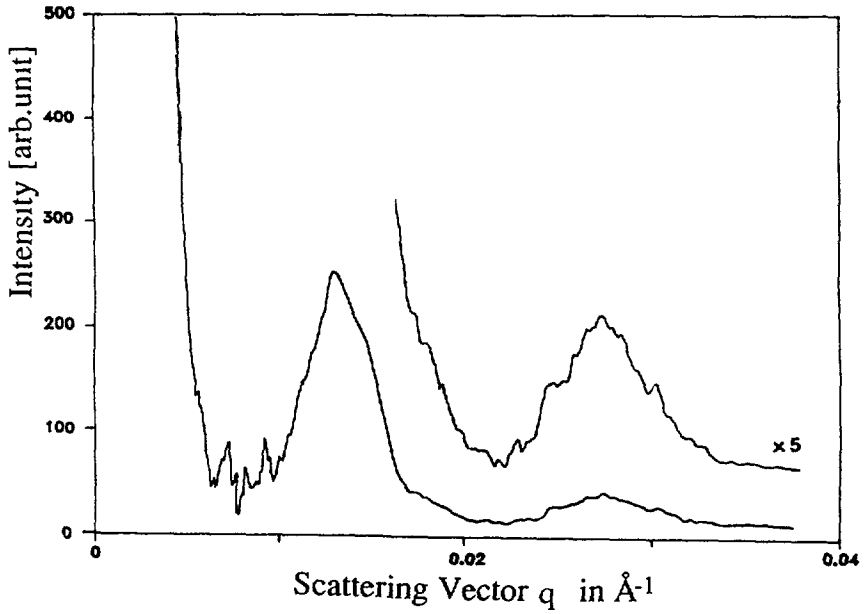

Fig. 11. — Scattering from swollen lamellar phases of fluorocarbon surfactant in water. The first two peaks have the same width.

figure 11. While the scattering peaks are clearly larger than the resolution of our camera, as is shown by the scattering of rat tail collagen, the two reflections showed the same width and there was no intense scattering in the center : thermal disorder (of the first type as introduced by Guinier) as well as substitution disorder (of the second type) can be ruled out in this case. The peak broadening is due to the small size of the crystallites. The high value of the bending rigidity of these highly charged stiff bilayers induces probably a large concentration of defects : the average distance between defects is of the order of 2 000 Å, because the FWHM broadening of the peaks is 4×10^{-3} Å^{-1}. The periodicity of the lamellar liquid crystal obtained is 490 Å : the typical extension of domains with the same director direction has therefore be determined by this experiment to be of the order of ten liquid crystal periods.

4.6 SCATTERING OF MONODISPERSE COLLOIDAL SILICA GELS. — Concentrated solutions of silica particles of diameter 3 200 Å form gels made by close packed particles in water up to a concentration (55 %) where a transparent glass is formed. The gel stabilisation is mainly due to electrostatic repulsions. This system provided by Persello and studied by Cabane and coworkers [60] has been chosen here to show a deconvoluted scattering curve $I(q)$ obtained with our multiple crystal camera. The volume fraction of particles in the sample used for figure 12 is 20 %. The strong repulsive interaction peaks dominate the scattering : the low scattering obtained for low angles is typical of a strongly repulsive colloidal system and disappears when salt of the order of 0.01 M is added to the sample. The width of the interaction peaks is related to the ratio of thermal energy to repulsive electrostatic interaction between particles.

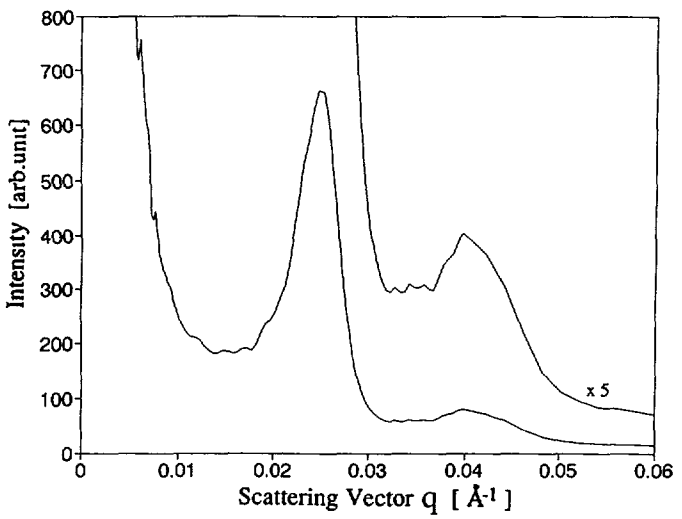

Fig. 12. — Scattering from a concentrated colloidal solution of silica in water. The spheres are 0.32 μm in diameter, their volume fraction is 20 %.

Conclusion.

A comparison of the performances and uses of a focusing camera and a multiple crystal camera is given in the table below [61].

	Multiple crystal camera	Focusing camera
major advantages	resolution q-independent resolution λ-independent	all points sampled in 2D together 2D detection allows anisotropic samples
main limitations	surface perturbated crystal chemical etching resistance to incoming flux	natural divergence of beam penumbra of main slits count-rate of available detectors

The possibilities offered by this type of camera are very promising for colloidal samples of typical sizes of the order of 1 000 Å : for smaller samples or periodicities, a focusing camera as introduced by Guinier is more efficient because all the data points are collected together. The limit between the two strategies can be evaluated practically at $q = 0.01$ Å^{-1} The domain where this type of double crystal multiple reflection setup as pioneered by Bonse and Hart is not yet obtainable by any other technique is the measurement of Bragg peak profiles, as this arrangement was used in order to investigate the power law decay near the Bragg peaks in lamellar liquid crystals stabilised by fluctuations [62].

The main drawback of the multiple reflection double crystal camera is the asymmetry of the collimation requiring systematic deconvolution procedures before obtaining interpretable decay laws of scattering. In order to avoid this problem, the so-called « crossed Bonse-Hart » geometry has been tested successfully on a storage ring at DESY for reflectivity studies [63-64] and for porosity studies [25]. A proposal exists to build a camera of this type as a public facility at ESRF, allowing for the first time access to weak X-ray scattering in the q-range around 10^{-3} Å^{-1} [65]. The resolution, set by the multiple reflection crystals, is independent of the wavelength used. This type of arrangement would make full use of the hard X-ray spectrum soon available at ESRF, because the rocking curve angular width decreases with the wavelength. So, a good penetration in colloidal samples would allow for sample thicknesses of several millimeters as in neutron scattering. The performance of multiple reflection arrangements for energies up to 50 keV has been recently thoroughly tested [66]. Moreover, the width of the rocking curve can be adjusted as well as the reflectivity or the beam size using asymmetrical multiple reflection crystals [28]. Wilkins has recently developed this technique introducing the design of condensing-collimating channel cut crystals [67]. The proposed « crossed Bonse-Hart » facility would allow for the first time quantitative scattering studies of emulsions, concentrated latex solutions and other systems of large industrial use available such as, sometimes metastable, concentrated solutions of large colloidal particles.

Acknowledgments.

We would like to thank Pr G. R. Strobl for making available to us his deconvolution routine, Dr Roberto Piazza for the fluorinated latexes, Dr Claudine Williams for the run at LURE, Pr A. Schmidt from the University of Missouri for the porous graphite sample, Dr M. Joanicot and Dr J. Persello from Rhône Poulenc for the dried silica gel sample and the colloidal solutions of silica, and finally, Montefluos Spa for the PFPE surfactant.

References

[1] GUINIER A., *Compt. rend. Acad. Sci.* **206** (1938) 1641-1643.

[2] LAMBARD J. and ZEMB T., 8th Int. meeting on small-angle scattering (Leuven 6-9 August 1990) *J. Appl. Cryst.* **24** (1991) 555-561.

[3] COMPTON A. H., *Phys. Rev.* **9** (1917) 29.

[4] COMPTON A. H. and ALLISON S. K., « X-rays in theory and experiment » (D. Van Nostrand Co., New York, 1935).
[5] DAVIS B. and STEMPEL, W., *Phys. Rev.* **17** (1921) 608-623.
[6] SLACK C. M., *Phys. Rev.* **27** (1926) 691-695.
[7] FANKUCHEN I. and JELLINEK M. H., *Phys. Rev.* **67** (1945) 201.
[8] DUMOND J. W. M., *Phys. Rev.* **72** (1947) 83-84.
[9] BEEMAN W. W. and KAESBERG P., *Phys. Rev.* **72** (1947) 512.
[10] KAESBERG P., RITLAND H. N. and BEEMAN W. W., *Phys. Rev.* **74** (1948) 71-73.
[11] GUINIER A. and FOURNET G., « Small angle scattering of X-rays » (John Wiley & Sons, 1955) p. 116-120.
[12] BONSE U. and HART M., *Appl. Phys. Lett.* **7** (1965) 238-240.
[13] BONSE U. and HART M., in « Small angle scattering » Syracuse 1965, H. Brumberger Ed. (Gordon and Breach Science Publ., 1966) and *Z. Phys.* **189** (1966) 151-162.
[14] IIDA A. and KOHRA K., *Phys. Status Solidi* **a 51** (1979) 533-542.
[15] RATAG V. M., SAKAI S. and WAKABAYASHI N., *Jpn. J. Appl. Phys.* **30** (1991) 1043-1044.
[16] KOVAL'CHUK M. V., KOV'EV E. K., KOZELIKHIN Y. M., MIRENSKII A. V. and SHILIN Y. N., *Instrum. Exp. Tech.* **19** (1976) 236-238.
[17] KOFFMAN D. M., *Adv. X-ray Anal.* **11** (1968) 332-338.
[18] ALS-NIELSEN J., LITSTER J. D., BIRGENEAU R. J., KAPLAN M., SAFINYA C. R., LINDEGAARD-ANDERSEN A. and MATHIESEN S., *Phys. Rev.* **B 22** (1980) 312-320.
[19] CHRISTENSEN F. E., HORNSTRUP A., JACOBSEN E., JONASSON P., MADSEN M. M., SCHNOPPER H. W., WESTERGAARD N. J. and ØRUP P., *Nucl. Instr. Meth. Phys. Res.* **A 256** (1987) 381-392.
[20] NAVE C., DIAKUN G. P. and BORDAS J., *Nucl. Instr. Meth. Phys. Res.* **A 246** (1986) 609-612.
[21] BORDAS J., MANT G. R., DIAKUN G. P. and NAVE C. J., *Cell Biology* **105** (1987) 1311-1318.
[22] FEWSTER P. F., *J. Appl. Cryst.* **21** (1988) 524-530, and *J. Appl. Cryst.* **22** (1988) 64-69.
[23] BONSE U., PAHL R. and NUBHARDT R., Hasylab annual report for 1986, 1987, Hamburg and *Acta Cryst.* **A 43** (1987) C-259.
[24] BONSE U., PAHL R., NUBHARDT R., KINNEY R. and PEKELA R. W., Hasylab annual report for 1988, edited by Hasylab in Hamburg, Germany.
[25] PAHL R., BONSE U., PEKALA R. W. and KINNEY J. H., 8th Int. Meeting on Small-Angle Scattering (Leuven, 6-9 august 1990) and *J. Appl. Cryst.* **24** (1971) 771-776.
[26] GUINIER A., « Théorie et technique de la radiocristallographie », troisième édition (Dunod, Paris 1964) Chap. 14.
[27] JAMES R. W., *Solid state Phys.* **15** (1963) 55-220.
[28] DEUTSCH M., *J. Appl. Cryst.* **13** (1980) 252-255 and *J. Appl. Cryst.* **13** (1980) 256-258.
[29] MATSUSHITA T., ISHIKAWA T. and KOHRA K., *J. Appl. Cryst.* **17** (1984) 257-264.
[30] LESIEUR P., LINDNER P., DESFORGES C., LAMBARD J. and ZEMB T., ICNS'91, *Physica B,* in press.
[31] LESIEUR P. and ZEMB T., « High resolution small angle X-ray scattering of colloids » in the Proceedings of the NATO ASI, June 11-21 1991 on « Structure and dynamics of supramolecular aggregates and strongly interacting colloids », S. H. Chen Ed. (Kluwer Acad. Publisher).
[32] The screens (Image Plate or IP) contain Eu^{3+} phosphorescent sites excited by X-rays and revealed by stimulated (blue) fluorescence excited by a red HeNe laser light. Our IP scanner is a « Phosphor Imager » developed by Molecular Dynamics Corporation USA. It allows the numerization of an image with a pixel size of 88 μm. The smaller image (one block) represents 256 × 228 pixels. The scanning is performed upon rectangular areas made of Nx.Ny blocks and the maximum image size, which is limited by the size of both the plate and the scanner, is 36 × 42 cm^2 (16 × 22 small blocks or 4 096 × 5 016 pixels). Scanning an IP after exposition to a 140 μm diameter 8 keV X-ray spot leads to a very narrow peak on the digitized image. Horizontal and vertical cuts of the latter and passing through the pixel of maximum intensity show a very fast decrease and a half width at 1 % of maximum of less than 5 pixels (or 6 pixels at 0.1 % of maximum). The background is about 0.5 count (≈ 8 keV) per pixel but it increases with time for long exposures. Exposure followed by a delayed read out of a signal shows a

decrease relative to read out performed just after exposure with two characteristic time constants. The first is about 30 min and represents 20 % of the signal while the second is about one week. The linearity range covers 6 orders of magnitude.

[33] KRATKY O., POROD G. and KAHOVEC L., *Z. Elektrochem.* **55** (1951) 53-59.

[34] SCHMIDT P. W. and HIGHT R. Jr., *Acta Cryst.* **13** (1960) 480-483.

[35] LAKE J. A., *Acta Cryst.* **19** (1967) 938-942.

[36] DEUTSCH M. and LUBAN M., *J. Appl. Cryst.* **11** (1978) 87-97.

[37] DEUTSCH M. and LUBAN M., *J. Appl. Cryst.* **11** (1978) 98-101.

[38] LUBAN M. and DEUTSCH M., *J. Appl. Cryst.* **13** (1980) 233-243.

[39] DEUTSCH M. and LUBAN M., *J. Appl. Cryst.* **20** (1987) 179-181.

[40] SCHMIDT P. W. and FERODOV B. A., *J. Appl. Cryst.* **11** (1978) 411-416.

[41] GLATTER O., *Acta Phys. Austriaca* **47** (1977) 83-102 and *J. Appl. Cryst.* **10** (1977) 415-421.

[42] GLATTER O., « Data treatment » in « Small angle scattering », O. Glatter and O. Kratky Ed. (Acad. Press, 1982).

[43] GLATTER O., private communication.

[44] STROBL G. R., *Acta Cryst.* **A 26** (1970) 367-375.

[45] DOYLE B. B., HUMES D. J. S., MILLER A., PARRY D. A. D., PIEZ K. A. and WOODHEAD-GALLOWAYJ, *Proc. R. Soc. London* **B 187** (1974) 37-46.

[46] HANSEN J. P., MC DONALD I. R., « Theory of simple liquids », 2nd ed. (Acad. Press, 1986).

[47] HAYTER J. and PENFOLD J., *Molec. Phys.* **42** (1981) 109-118.

[48] MAGID L. J., *Colloids and Surfaces* **19** (1986) 129-158.

[49] CHEVALIER Y. and ZEMB T., *Rep. Progr. Phys.* **53** (1990) 279-371.

[50] PIAZZA R., STAVANS J., BELLINI T., LENTI D., VISCA M. and DEGIORGIO V., *Progr. Colloid. Polym. Sci.* **81** (1990) 89-94.

[51] DEGIORGIO V. and PIAZZA R., « Colloidal crystals made of anisotropic spherical particles : a quasielastic light scattering study » in the Proceedings of the NATO ASI, June 11-21 1991 on « Structure and dynamics of supramolecular aggregates and strongly interacting colloids », S. H. Chen Ed. (Kluwer Acad. Publisher).

[52] CHACHATY C., KORB J. P., VAN DER MAAREL J. R. C., BRAS W. and QUINN P., *Phys. Rev.* **B 44** (1991) 4778-4793.

[53] SCHMIDT P. W., *J. Appl. Cryst.* **24** (1991) 414-435.

[54] BALE H. D. and SCHMIDT P. W., *Phys. Rev. Lett.* **53** (1984) 596.

[55] SCHMIDT P. W., HOHR A., NEUMANN H. B., KAISER H., AVNIR D. and LIN J. S., *J. Chem. Phys.* **90** (1989) 5016.

[56] DWIGGINS C. W. Jr., *J. Appl. Cryst.* **12** (1979) 401-402.

[57] CHITTOFRATI A., LENTI D., SANGUINETI A., VISCA M., GAMBI C. M. C., SENATRA D. and ZHOU Z., *Progr. Colloid Polymer Sc.* **79** (1989) 218-222.

[58] DUBOIS M. and ZEMB T., *Langmuir* **7** (1991) 1352-1360.

[59] ZEMB T., BELLONI L., DUBOIS M. and MARCELJA S., submitted to *Progr. Colloid Polymer Sci.* (1991).

[60] CABANE B. *et al.*, in preparation.

[61] ALDISSI M., HENDERSON S. J., WHITE J. W. and ZEMB T., *Mat. Sc. Forum* **27/28** (1988) 437-444.

[62] ROUX D. and SAFINYA C. R., *J. Phys. France* **49** (1988) 307-318.

[63] APPEL A., BONSE U. and STAUDENMANN J. L., *Z. Phys.* **B 81** (1990) 371-379.

[64] BONSE U. and FISCHER K., *Nucl. Instr. Meth.* **190** (1981) 593-603.

[65] ZEMB T., LAMBARD J. LESIEUR P., BERNON R., ROUX D., BAROIS P., WILLIAMS C., STREY R. and WILKINS S., « Proposition pour un montage de diffraction à très haute résolution et très petits angles de type Bonse et Hart croisée à l'ESRF » CEA report n° R5523 (1990), available at : Service de Documentation, C.E.N. Saclay, F91191 Gif-sur-Yvette Cedex, France.

[66] SIDDONS G. B., RIEKEL C. and HASTINGS J. B., *J. Appl. Cryst.* **23** (1990) 401-405.

[67] WILKINS S. W. and STEVENSON A. W., « A class of condensing-collimating channel cut monochromators for SAXS, XRPD and other applications » (Elsevier Sci. Pub., 1988) p. 321-328.